applied sciences

IMPACT FACTOR 2.5

CITESCORE 5.3

Article

Machine Learning-Enhanced Discrimination of Gamma-Ray and Hadron Events Using Temporal Features: An ASTRI Mini-Array Analysis

Valentina La Parola, Giancarlo Cusumano, Saverio Lombardi, Antonio Alessio Compagnino, Antonino La Barbera, Antonio Tutone and Antonio Pagliaro

Special Issue

AI Horizons: Present Status and Visions for the Next Era

Edited by

Dr. Antonio Pagliaro and Dr. Pierluca Sangiorgi

MDPI

https://doi.org/10.3390/app15073879

applied sciences

MDPI

Article

Machine Learning-Enhanced Discrimination of Gamma-Ray and Hadron Events Using Temporal Features: An ASTRI Mini-Array Analysis

Valentina La Parola [1,2,*], Giancarlo Cusumano [1,2], Saverio Lombardi [2,3,4,*], Antonio Alessio Compagnino [1], Antonino La Barbera [1,2], Antonio Tutone [1,2] and Antonio Pagliaro [1,2,5,*]

1 INAF IASF Palermo, Via Ugo La Malfa 153, I-90146 Palermo, Italy; giancarlo.cusumano@inaf.it (G.C.); antonio.compagnino@inaf.it (A.A.C.); antonino.labarbera@inaf.it (A.L.B.); antonio.tutone@inaf.it (A.T.)
2 ICSC—Centro Nazionale di Ricerca in HPC, Big Data e Quantum Computing, I-40121 Bologna, Italy
3 INAF—Osservatorio Astronomico di Roma, Via Frascati 33, Monte Porzio Catone, I-00040 Rome, Italy
4 ASI—Space Science Data Center, Via del Politecnico, snc, I-00133 Rome, Italy
5 Istituto Nazionale di Fisica Nucleare Sezione di Catania, Via Santa Sofia, 64, I-95123 Catania, Italy
* Correspondence: valentina.laparola@inaf.it (V.L.P.); saverio.lombardi@inaf.it (S.L.); antonio.pagliaro@inaf.it (A.P.)

Abstract: Imaging Atmospheric Cherenkov Telescopes (IACTs) have revolutionized our understanding of the universe at very high energies (VHEs), enabling groundbreaking discoveries of extreme astrophysical phenomena. These instruments capture the brief flashes of Cherenkov light produced when VHE particles interact with Earth's atmosphere, providing unique insights into cosmic accelerators and high-energy radiation sources. A fundamental challenge in IACT observations lies in distinguishing the rare gamma-ray signals from an overwhelming background of cosmic-ray events. For every gamma-ray photon detected from even the brightest sources, thousands of cosmic-ray-induced atmospheric showers trigger the telescopes. This profound signal-to-background imbalance necessitates sophisticated discrimination techniques that can effectively isolate genuine gamma-ray events while maintaining high rejection efficiency for cosmic-ray backgrounds. The most common method involves the parametrization of the morphological feature of the shower images. However, we know that gamma-ray and hadron showers also differ in their time evolution. Here, we describe how the pixel time tags (i.e., the record of when each camera pixel is lit up by the incoming shower) can help in the discrimination between photonic and hadronic showers, with a focus on the ASTRI Mini-Array Cherenkov Event Reconstruction. Our methodology employs a Random Forest classifier with optimized hyperparameters, trained on a balanced dataset of gamma and hadron events. The model incorporates feature importance analysis to select the most discriminating temporal parameters from a comprehensive set of time-based features. This machine learning approach enables effective integration of both morphological and temporal information, resulting in improved classification performance, especially at lower energies.

Keywords: machine learning; ensemble learning; imaging atmospheric Cherenkov telescopes; gamma/hadron separation; image analysis; pattern recognition

Academic Editor: Pedro Couto

Received: 21 February 2025
Revised: 25 March 2025
Accepted: 26 March 2025
Published: 1 April 2025

Citation: La Parola, V.; Cusumano, G.; Lombardi, S.; Compagnino, A.A.; La Barbera, A.; Tutone, A.; Pagliaro, A. Machine Learning-Enhanced Discrimination of Gamma-Ray and Hadron Events Using Temporal Features: An ASTRI Mini-Array Analysis. *Appl. Sci.* **2025**, *15*, 3879. https://doi.org/10.3390/app15073879

1. Introduction

The ground-based observation of Gamma rays from celestial sources has been made possible in the last 40 years thanks to the development of the Imaging Atmospheric

Cherenkov Telescope (IACT) technique [1], which exploits the Cherenkov effect to detect gamma photons by observing the effects of their passage through the atmosphere. Specifically, when gamma rays with energies above a few tenths of GeVs (VHE—Very High Energy) reach the Earth's atmosphere, they start a shower of secondary charged particles traveling with a velocity higher than the light speed in the atmosphere [2]. This produces a perturbation in the atmosphere's atoms and molecules that in turn emit a faint blue-ultraviolet radiation as they regain their equilibrium. This radiation, which comes as an extended pool of light in the ∼250–900 nm wavelength range, can be detected by large-field optical telescopes with appropriate ultra-fast electronics since the Cherenkov flash lasts only a few ns. Therefore, we do not directly observe the primary photon, but we collect the footprint of its interaction with the atmosphere, which has the shape of an approximate ellipsoid extended on a few degrees of arc. The information on the incoming direction and on the energy of the primary Gamma photon can be reconstructed with appropriate image analysis techniques. The use of an array of several telescopes observing simultaneously the same sky direction improves the IACT technique, since the detection of the same shower by more than one telescope allows for an accurate triangulation of the incoming direction and for a better determination of the energy of the primary gamma-ray photon.

Although the IACT technique is the most effective one for the observation of VHE sources, its sensitivity is heavily affected by the overwhelming background of charged cosmic rays (relativistic nuclei and particles from the outer space) that also ignite an atmospheric cascade with the production of Cherenkov light: in the exemplar case of the Crab Nebula, one of the brightest persistent sources in the gamma-ray sky, the photon rate in the relevant energy range is about three orders of magnitude lower than the cosmic-ray rate. It is thus of paramount importance to find an efficient method to separate the images generated by gamma-ray photons from those generated by cosmic-ray primary particles that are not related to the primary target. Usually, this is conducted by exploiting the morphological diversity among images with different origin [3]: the image of a shower initiated by a gamma-ray photon has quite a regular elliptical shape, while a hadronic shower typically has a more irregular shape. This difference can be exploited using a consolidated set of parameters with good discriminating efficiency, and modern data processing software that makes large use of machine learning method (see, e.g., [4] and reference therein).

We know, however, that gamma and hadronic showers differ also for their time evolution [5,6]. This characteristic can be used, coupled with the morphological parametrization, to improve the hadron rejection (see, e.g., Figure 1, where two showers with a very similar morphology show a visibly different time structure). However, the space of possible parameters derived from the image time characterization has not been fully explored in the context of ASTRI data reconstruction, although time parameters have been extensively studied and used for nearly two decades in the analysis of IACT data (see, for example, [7]). The aim of this paper is to describe a set of several time parameters developed and tested for the case study of the ASTRI Mini-Array telescopes [8], which are being installed at the *Observatorio del Teide*, in the Canary Islands (Spain), in order to evaluate their effectiveness for the gamma/hadron discrimination.

This work presents several key innovations in gamma-ray/hadron discrimination for Imaging Atmospheric Cherenkov Telescopes (IACTs). While previous approaches have primarily relied on morphological and stereoscopic parameters, our study introduces three significant advances:

1. **Novel Integration of Temporal Features:** We develop and implement a comprehensive temporal parameter selection methodology specifically optimized for the ASTRI Mini-Array telescope system. This approach goes beyond traditional timing

measurements by incorporating eight carefully selected temporal parameters that capture various aspects of shower evolution.

2. **Enhanced Discrimination Framework:** Our work introduces a specialized Random Forest implementation that combines both conventional morphological parameters and temporal features. This hybrid approach enables more robust discrimination between gamma-ray and hadron events, particularly in the challenging low-energy regime (below ∼1.5 TeV).
3. **Quantifiable Performance Improvement:** The integration of our temporal parameter selection methodology demonstrates a significant enhancement in discrimination ability, improving the quality factor from 3.32 (using only morphological parameters) to 3.68 (with selected temporal parameters). This represents approximately a 10.8% improvement in separation performance.

These advances are particularly significant for the ASTRI Mini-Array context, where optimizing event discrimination directly impacts the telescope array's ability to detect and characterize very high-energy gamma-ray sources. Our approach not only improves discrimination performance but also provides a framework for incorporating temporal information that can be adapted for other IACT systems.

In the next subsections, we put our work in the context of the present Cherenkov experiments, with particular focus on the ASTRI Mini-Array, and on the state of the art of the use of time parameters in the Cherenkov data analysis. In Section 2, we describe the data samples considered in this work, while in Section 3, we describe the standard procedure by which we achieve the gamma/hadron separation for our data. In Section 4, we describe the set of parameters developed and tested for this work, and in Section 5, we describe the selection of the most promising ones. In Section 6, we report our performance results on their effectiveness in the Cherenkov data analysis. In Section 7, we outline our conclusions and future prospects.

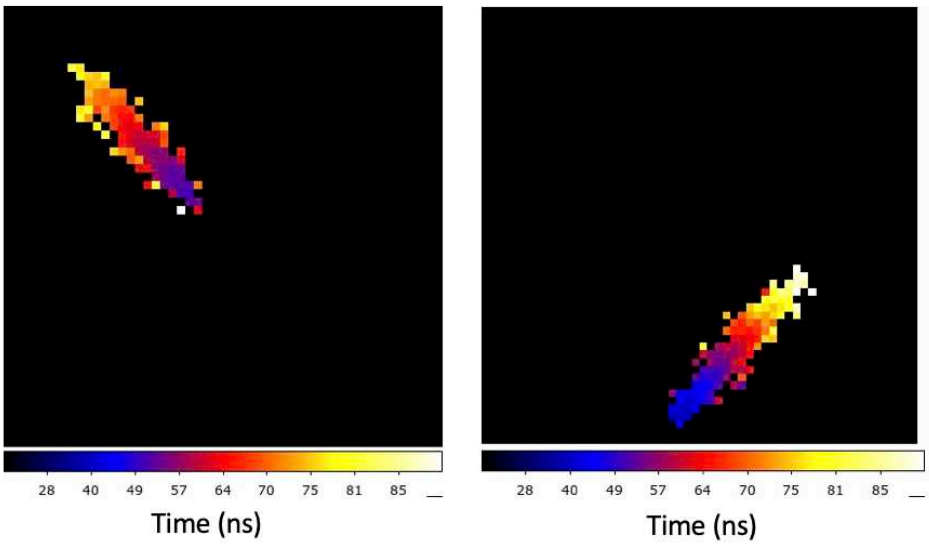

Figure 1. Simulated Cherenkov shower images as observed by an ASTRI Mini-Array telescope, illustrating the differences in time evolution between different types of events. The image covers the entire ASTRI field of view (each side spanning approximately 10 deg). The color scale indicates the time when the pixel is triggered by the incoming Cherenkov photons (see Section 2.3 for details on the time recording process), with the black, indicating that the pixel has not been triggered. The time (in ns) increases from blue to white. In this example, the gamma-initiated event (**left**) evolves slowly than the hadron-initiated event (**right**).

1.1. The ASTRI Mini-Array

The ASTRI (*Astrofisica con Specchi a Tecnologia Replicante Italiana*) Mini-Array [8] is an international project led by the Italian National Institute for Astrophysics (INAF) to build and operate an array of nine 4-m class IACTs at the *Observatorio del Teide* (Tenerife, Spain). The array is designed to be sensitive to energies in the 1–200 TeV energy range, and to achieve an angular resolution of $\sim 3'$, and an energy resolution of $\sim$10% above about 10 TeV [9].

The primary scientific objective of the project is to advance gamma-ray astronomy at TeV and multi-TeV energy scales, contributing to a deeper understanding of topics such as the origin of cosmic rays, the extra-galactic background light (EBL), and other fundamental physics questions. They also focus on time-domain and multi-messenger astrophysics at the TeV and multi-TeV energy scales, as well as on the detection and study of gamma-ray bursts and multi-messenger transients in the very high-energy (VHE) domain. Additionally, the ASTRI Mini-Array will conduct stellar intensity interferometry studies. More information on the ASTRI Mini-Array Core Science program can be found in the dedicated paper by the ASTRI Collaboration [10].

The first telescope of the ASTRI Mini-Array has been completed and is now in its commissioning phase. Within 2025, two more telescopes out of the planned nine will be operative on site. As of today, the prototype telescope ASTRI-Horn [11–13] is fully operational at the *Osservatorio Astrofisico* "M.G. Fracastoro" on Mount Etna. The prototype is used mostly for calibration and test purposes (together with a good fraction of time dedicated to scientific observation). The Mini-Array telescopes will feature some significant differences with respect to the ASTRI-Horn setup, among which (and of interest for this paper) we mention the implementation of the pixel time tag readout (see Section 2).

1.2. Event Reconstruction

The images collected by IACTs are the indirect signature (mostly in the ultraviolet wavelength band) of the interaction of a VHE photon (or charged particle) with the atmosphere. The data need to be processed to reconstruct the energy and the arrival direction of the primary event and to discriminate between photon- and hadron-initiated events. To this aim, several reconstruction steps are required, after the Cherenkov signals recorded by the telescopes' cameras have been fully calibrated [14].

- **Image Cleaning.** The main sources of noise in the images collected by the telescope's camera are the night sky diffused background light, electronic noise, and other signals not related to Cherenkov radiation (e.g., stars). These must be removed in order to isolate the Cherenkov shower image.
- **Image Parameterization.** Each atmospheric shower produces a unique Cherenkov light signature due to the complex cascade of particle interactions in the atmosphere. To analyze these distinctive patterns, we employ a comprehensive set of morphological parameters that capture essential features such as the shower's geometric properties and the spatial distribution of Cherenkov light across the camera plane.
- **Stereo Reconstruction.** When the same shower is observed by more than one telescope, the information from multiple detectors can be combined in order to reconstruct the full 3D trajectory of the incident primary.

Random Forest Classification Method

For gamma/hadron discrimination, we employ the Random Forest algorithm, a powerful ensemble learning technique particularly well-suited for classification problems in astroparticle physics. This method is implemented in the ASTRI data reduction and sci-

entific analysis software package (A-SciSoft v0.7.4) [14], establishing our benchmark for performance evaluation.

Random Forest [15] operates by constructing multiple decision trees during training, with each tree built from a bootstrap sample (known as "bagging") of the training data. The algorithm introduces randomness by considering only a subset of features at each split point—a technique known as the random subspace method. This approach ensures diversity among trees and reduces correlation between them, thereby enhancing the generalization ability of the ensemble.

The combined analysis of morphological parameters and stereoscopic data yields a detailed characterization of each event. Through this machine learning approach, we derive both a classification parameter (gammaness) indicating the likelihood of the event being gamma-ray-induced and an estimate of the primary particle's energy. For classification tasks such as distinguishing gamma-ray events from hadronic backgrounds, the final prediction is determined by majority voting across all trees, while for regression problems (such as energy estimation), it uses the average of the predictions.

The strength of Random Forest lies in combining numerous "weak learners" (individual decision trees) into a robust "strong learner" (the forest). Each tree captures different patterns in the data, and their collective wisdom provides superior predictive performance compared to any individual tree. For our gamma/hadron separation task, this ensemble approach effectively handles the complex, high-dimensional feature space created by both morphological and temporal shower parameters.

Random Forests provide several key advantages over traditional decision trees:

- **Reduction in Overfitting**: By averaging the predictions of multiple trees, the Random Forest mitigates the risk of overfitting that is often associated with individual decision trees.
- **Robustness**: The aggregation of multiple trees' predictions leads to more stable and reliable outputs, making the model robust to noise and variations in the data.
- **Feature Importance**: Random Forests inherently provide a measure of feature importance, allowing for insights into which features are most influential in the prediction process. This capability proves particularly valuable when evaluating the relative contribution of temporal features compared to traditional morphological parameters.

We are aware that more advanced Machine Learning techniques could potentially perform better than Random Forest in this context. However, our aim here is to assess whether the introduction of time parameters in the analysis procedure provides a significant performance boost over the standard method based only on morphological and stereo parameters, and for a fair comparison, we will maintain the use of Random Forest as already implemented in the ASTRI analysis software A-SciSoft v0.7.4. The optimization of the method, including the test of different ML techniques and the use of real data from the ASTRI-1 telescope, will be the subject of a forthcoming paper.

1.3. Time Parameters in IACTs: State of the Art

Beyond the information derived from light intensity, the arrival time of Cherenkov photons on the camera represents another valuable data dimension. This temporal information depends on the geometry of the particle shower, the impact distance of the telescope, and the altitude of photon emission. The incorporation of time information enhances the overall performance of Cherenkov telescopes, improving sensitivity, resolution, and energy threshold capabilities. Here, we delve into various applications of time information in the analysis of Cherenkov telescope data.

- Image Cleaning. **In the case of the MAGIC telescopes, the standard image cleaning procedure has been enhanced by incorporating temporal constraints alongside the**

traditional intensity-based selection. This refined approach exploits the expectation that pixels belonging to the shower image light up within a few tens of nanoseconds, thereby effectively suppressing contributions from night sky background fluctuations and other spurious signals [16]. **The adoption of this method, particularly after the introduction of a 2 GS/s digitization system capable of recording the full waveform of pixel signals, resulted in a significant background reduction by a factor of two and an improvement in sensitivity by a factor of 1.4 for point-source observations** [7,17].

- Time Parameters. Quantities characterizing the temporal profile of the image, such as time gradient and time RMS, serve as additional inputs (independent of the purely morphological features) for discriminating hadron-generated signals and estimating energy and impact distance. Integration of these parameters into the analysis of the MAGIC telescope data led to a halving of the residual hadronic background while maintaining the same number of excess events compared to an analysis using only standard parameters [7].
- Deep Learning Techniques. The use of deep learning, an artificial intelligence technique employing convolutional neural networks, presents a promising avenue for classifying Cherenkov telescope images based on both charge and time information. This approach involves creating two-dimensional maps of pixels containing various waveform parameters, which, alongside the intensity map, significantly improves event classification. Tested on simulated data for the future Cherenkov Telescope Array (CTA), this method exhibited promising results for discriminating proton and electron backgrounds [18].

Apart from MAGIC, other notable Cherenkov telescopes, such as VERITAS (Very Energetic Radiation Imaging Telescope Array System) [19] and HESS [20], have also demonstrated the efficacy of incorporating time information into their data analyses. These telescopes, like MAGIC, have explored the implementation of advanced algorithms for image cleaning and the extraction of time parameters, contributing to the refinement of background discrimination and sensitivity.

The integration of time information into Cherenkov telescopes' data reconstruction proves to be a versatile and advantageous technique. Its implementation across various telescopes showcases its adaptability and potential for enhancing the precision and reliability of astrophysical observations. This technique, particularly beneficial for single telescopes lacking stereoscopic vision of particle showers, underscores the significance of time as an additional parameter for reconstructing events.

In this paper, we focus on the definition, evaluation, and application of time-derived parameters for Gamma/Hadron separation in the context of the ASTRI Mini-Array.

2. Data

2.1. Data Samples and Simulation Procedure

The inherent probabilistic nature of Cherenkov radiation necessitates a statistical approach to reconstructing primary gamma-ray characteristics. Modern analysis relies on sophisticated Monte Carlo (MC) simulations that model both the atmospheric particle cascade and the subsequent detector response.

Our simulation framework generates extensive particle event catalogs by sampling from probability distributions that define the fundamental properties of incoming particles—their energies, trajectories, and particle types. Each simulated event initiates an atmospheric cascade, producing a detailed model of secondary particle production and the resulting Cherenkov light distribution.

For this analysis, we utilized the comprehensive *ASTRI MA Prod2-Teide* simulation dataset [9], which encompasses the following:

- 4×10^7 on-axis gamma-ray events;
- 2×10^8 diffuse electron events;
- 2×10^9 diffuse proton events.

These events were simulated over an area encompassing all nine ASTRI Mini-Array telescopes at the Teide site. The simulation incorporates site-specific parameters, including geographical coordinates, elevation, atmospheric conditions, and precise telescope positions. Observations were modeled at 20-degree zenith angles, with dedicated simulations for both northward and southward pointing directions.

The energy coverage spans 0.1–330 TeV for gamma-rays and electrons, extending to 600 TeV for protons. While we employed a spectral index of -1.5—flatter than observed spectra [9]—to ensure adequate statistics at high energies, our differential analysis methodology incorporates appropriate event weights to accurately reflect the physical energy distributions of each particle species.

The simulation pipeline consists of two primary stages:

1. **Atmospheric Shower Development:** Using the Corsika software package 7.7550 [21], we model the complete evolution of particle cascades through the atmosphere, generating detailed maps of the Cherenkov light distribution at ground level.
2. **Telescope Response Simulation:** The sim_telarray package [22] models the interaction between the Cherenkov photons and telescope systems, including optical ray-tracing and detector response characteristics, producing realistic shower images as captured by the telescope cameras.

2.2. Data Levels

The data format of the ASTRI project was originally defined in compliance with those of the Cherenkov Telescope Array, adopting the FITS format [23]. Detailed information on the levels of the ASTRI data processing can be found in [14]. ASTRI data levels of interest for the work presented here are as follows:

- Data Level 1a (DL1a): Single-telescope calibrated event data. For each event, they contain intensity and time tag uncleaned images to be processed for the evaluation of morphological and time parameters; they are used as input in our tests;
- Data Level 2a (DL2a): Array-wise event parameter data. For each event, they contain the morphological and time-based parameters for all the telescopes in the array triggered by that event, plus its stereoscopic reconstruction parameters. At the moment, all data level files are produced with standard procedure implemented in`A-SciSoft`, except for the computation of the time parameters at DL2a, which is currently performed with a working-code being implemented in the standard data reconstruction chain;
- Data Level 2b (DL2b): Array-wise fully reconstructed files. For each event, they contain the final global reconstructed parameters, which define the probability to be a gamma-ray event, and its reconstructed energy and arrival direction in the sky.

In this work, we considered two DL2b data samples: the first was achieved by reducing data up to DL2b without any time-based parameters as training parameters in the Random Forest method for gamma/hadron separation, while the second by including in the Random Forest procedure, in addition to the standard ones, the time-based parameters described in Section 4.

The DL2b files of the two data samples are then further processed, separately, using appropriate tools of the ASTRI data reduction and scientific analysis software in order to derive the global properties of the final dataset in terms of sensitivity, angular resolution,

and energy resolution. In this way, we are able to assess the impact of the time parameters in the final performance of the system.

2.3. Pixel Time Readout in the ASTRI Mini-Array Camera

IACTs are equipped with a trigger system, capable of reacting in a ns time scale to the Cherenkov flash, activating the camera readout. The details on the camera pixel trigger and readout system for the ASTRI Mini-Array telescopes can be found in Sottile et al. [24]. For the purpose of this paper, it is important to report that a topological trigger occurs when a minimum number N of adjacent pixels reach a predefined charge threshold T (corresponding to a minimum number of photoelectrons due to Cherenkov photons recorded simultaneously by each pixel). Both N and T are set for each observing run according to the actual observing conditions, with $N \geq 4$, and $T \gtrsim 7$ (as for the MC production used in this study). The topological trigger signal is sent to the back-end electronics that enable the camera trigger and, eventually, the readout of the entire camera.

Each pixel is then assigned a value between 0 and 255 that represents the time (in ns) when the cumulative charge readout in the pixel exceeds the charge threshold T, with the camera trigger set at time 128. The value 255 is assigned to pixels reading a signal below the threshold T for the entire duration of the time register readout process (lasting 255 ns and centered on the camera trigger time). The pixel time information is stored in the DL1a files with the same array structure as the intensity image and can be processed and used as an image as well.

3. Basic Settings for Gamma/Hadron Separation

We describe here how our tests were incorporated in the already existent analysis software `A-SciSoft`, developed for the analysis of the data collected by ASTRI Mini-Array and ASTRI-Horn.

In the benchmark configuration, `A-SciSoft` employs a Random Forest algorithm applied to a set of morphological and stereoscopic parameters (see Section 3) to provide a "gammaness" indicator for the gamma/hadron separation and to reconstruct the shower energy and arrival direction. For our tests, we use the same tool, adding a set of several time parameters to the morphological parameter set.

The feature importance scores generated by the Random Forest model guided our selection of the most relevant parameters, further optimizing the performance of our classification algorithm.

To optimize the classifier's performance, we implemented a systematic data balancing strategy based on the shower size parameter $log_{10}(SIZE)$ (SIZE represents the total photoelectron content in the cleaned image, as detailed in Section 3). We partitioned the full dataset into 100 logarithmic SIZE bins and applied selective pruning to achieve equal representation of gamma and hadron events within each bin.

Our initial dataset comprised the following:

- 136,498 gamma-ray events;
- 126,645 hadron events.

The pruning algorithm selectively removed:

- 14,204 gamma-ray events;
- 4351 hadron events.

This process yielded a perfectly balanced final dataset containing 122,294 events of each type. This careful equilibration across the SIZE parameter space serves two crucial purposes: it prevents classification bias that could arise from uneven event distributions, and it ensures robust performance across the full range of shower intensities. Such balancing

is particularly important for machine learning applications in gamma-ray astronomy, where classification accuracy must be maintained across multiple orders of magnitude in shower size.

Hyperparameter tuning was performed by means of a randomized search that implements a "fit" and a "score" method.

Our implementation employs a carefully optimized set of hyperparameters, selected to balance computational efficiency with classification performance:

- **Ensemble Size** (*n_estimators* = 100): We deployed a forest of 100 decision trees, representing an optimal compromise between model complexity and predictive power. While larger ensembles were tested, we observed diminishing returns beyond this size, with minimal performance gains from hundreds of trees and prohibitive computational costs from thousands.
- **Feature Sampling** ($max\_features = \sqrt{n_{features}}$): At each decision node, the algorithm considers a subset of features equal to the square root of the total feature count, promoting diversity in the decision-making process.
- **Tree Architecture**:
  - *max_depth* = 20: limits each tree's maximum depth to prevent overfitting while maintaining sufficient model complexity;
  - *min_samples_split* = 2: Requires at least two samples to justify further node splitting;
  - *min_samples_leaf* = 2: Ensures each terminal node contains at least two samples.
- **Sampling Strategy** (*bootstrap* = True): Implements bootstrap aggregating (bagging) during tree construction, where each tree trains on a randomly sampled subset of the data. This approach enhances model robustness and reduces overfitting by introducing diversity in the training process.

This configuration achieves an effective balance between model complexity, computational efficiency, and classification performance across our gamma-hadron discrimination tasks.

Morphological and Stereoscopic Parameters

The analysis of Cherenkov radiation events captured by the ASTRI Mini-Array demands a comprehensive parameterization framework that encapsulates both the spatial and temporal characteristics of the atmospheric showers. Each event reconstruction relies on multiple complementary parameters that collectively characterize the fundamental properties of the primary particle interaction and subsequent shower development.

In our study, we have utilized the main morphological and stereoscopic parameters commonly adopted in Cherenkov analysis [3] and already included in the standard analysis procedure of `A-SciSoft`.

Our analysis framework incorporates the following key parameters to characterize Cherenkov shower images:

- **Shower Size Parameters**:
  - $\log_{10}(SIZE)$: Logarithmic measure of the total photoelectron content in the cleaned image;
  - $DENS$: Compactness measure defined as $\log_{10}(SIZE/(WIDTH \times LENGTH))$;
  - $CONC$: Image concentration, computed as the ratio between the two brightest pixel intensities and total shower size.
- **Shape Parameters**:
  - $WIDTH$: Minor axis of the best-fit shower ellipse [3];
  - $LENGTH$: Major axis of the best-fit shower ellipse [3];

  - *M3LONG*: Third-order moment characterizing image elongation.
- **Image Structure Metrics**:
  - *LEAKAGE*: Ratio of edge pixel signals to total shower size;
  - *NUMCORE*: Count of shower core pixels [14];
  - *NUMBOUNDARY*: Count of shower boundary pixels [14];
  - *NUMISLAND*: Number of isolated pixel clusters (used for filtering).
- **Stereoscopic Reconstruction Parameters**:
  - *NUSEDTEL*: Number of telescopes contributing to stereoscopic reconstruction;
  - *TELIP*: Distance between reconstructed shower core and telescope position;
  - *STMAXH*: Reconstructed height of shower maximum.

To carry out our tests, we have added to this set a different subset of the temporal parameters described in Section 4.

4. Time Parameters

We describe here the implementation of the parameters we have derived from the pixel time tags. The time parameters are evaluated after a standard cleaning procedure [14]: we use only the time tags recorded for the pixels survived in the cleaned image. In the following, t_p is the time recorded in each pixel (TTP), i_p is the charge intensity in each pixel, and n_p is the total number of pixels in the cleaned image.

4.1. Standard Time Parameters

These are the two main time parameters present in the literature (see, e.g., the ones in use for the analysis of the MAGIC telescopes data [7]).

Time RMS. It is a measure of the spread of the TTPs and it is totally independent of the image morphology and position on the camera. For each cleaned image, we derive the Root Mean Square of the pixel time tags as follows:

$$T\_RMS = \sqrt{\sum (t_p - t_{AVG})^2} \tag{1}$$

where t_{AVG} is the average pixel time, evaluated as $t_{AVG} = \frac{\sum t_p}{n_p}$.

Time Gradient. It measures how fast the shower image evolves along the image major axis. The image is reduced to one dimension by projecting the pixel coordinates onto the major axis. The gradient is defined as the first order coefficient b of the quadratic function $t = ax_p^2 + bx_p + c$ that best fits the arrival times versus the space coordinate along the major axis (x_p).

4.2. Parameters Based on the Time RMS

Normalized Time RMS. It provides a normalized measure of the temporal dispersion. The RMS is evaluated as usual (see definition above), and then divided by the size of the cleaned image ($SIZE = \sum i_p$) and the number of pixel (n_p):

$$T\_RMSNORM = \frac{T\_RMS}{SIZE * n_p} \tag{2}$$

Weighted Time RMS. This parameter would put in evidence any effect in the time dispersion related to the pixel charge content. The average time is evaluated by weighing each pixel time for the signal intensity recorded in the relevant pixel. Thus: $t_{AVGW} = \sum (t_p \times i_p)/SIZE$. In the evaluation of the RMS, a fourth root is used instead of a square root in order to enhance the separation effect.

$$T\_RMS\_W = ^4 \sqrt{\sum (t_p - t_{AVGW})^2 / n_p^3} \quad (3)$$

Linearized Time RMS. It measures the dispersion of the pixel time tags with respect to the line that describes the shower time evolution along the image

$$T\_RMS\_L = \sqrt{\sum (t_p - bx_p - c)^2 / n_p^2} \quad (4)$$

where b and c are the same coefficients derived for the time gradient.

4.3. Parameters Based on the Time-Size or Time-Distance Dispersions

We have explored the Pixel Size-Time (ST space) and Pixel Distance-Time (DT space) parameter spaces (where pixel size is the charge content i_p of the single pixel and distance is intended as between each pixel and the image baricenter) searching for features that could be significant for the Gamma/Hadron discrimination. The latter space describes how the shower image evolves in time (i.e., at which distance from the image centroid the pixels light up first); the former tells if brighter pixels are faster to trigger. We can then apply to these plots a morphological analysis using the same algorithm as for the Hillas parameters (algorithms are described in [25]), to evaluate a width and a length for these dispersions. The quantities considererd for further analysis are width and length in the ST space (both in a simple form and normalized for the total SIZE of the image and the number of pixel n_p: WID_ST, LEN_ST, WID_ST_NORM, and LEN_ST_NORM) and length in the DT space (LEN_DT).

This concept can be expanded to 3-dimensional space. In particular, we have explored the two spaces defined by X and Y coordinates of the pixel plus pixel time (XYT space), and Pixel Size-Time-Pixel Distance (STD space) for each pixel, obtaining a width and a length. Here, we have examined the length and the width in the STD space (LEN_SDT, WID_SDT) and the length in the XYT space (LEN_XYT).

4.4. Other Parameters

Lacunarity. Lacunarity was initially conceived to characterize fractals (Mandelbrot [26], Lin and Yang [27], Gefen, Meir, and Aharony [28]), as it reveals variations in their space-filling structures, with lower lacunarity implying greater visual uniformity. In our case, lacunarity is used to quantify heterogeneity in the timing of showers. We use the gliding box method described in Allain and Cloitre [29]. We consider a gridded timeline, with each cell corresponding to 1 ns. If any pixel has time tag t_p, the cell corresponding to t_p on the timeline is assigned a 1, otherwise the cell is marked with a zero. A sliding box of size n_M (>4, it can be adjusted to optimize the result) is shifted over the timeline grid, and at each step, the mass M of the box (i.e., the number of non-zero cells) is recorded. The frequency distribution of M is converted into a probability distribution P_M across the number of gliding boxes, and the lacunarity is computed using the variance and mean of the number of full cells per gliding box, as

$$T\_LAC = \frac{\mathrm{Var(P_M)}}{\mathrm{Avg(P_M)}^2} + 1 \quad (5)$$

This results in values between 1 and ∞, with 1 indicating a uniform dispersion of full cells at a given scale, and values different from 1 signifying non-uniformity in the distribution. Our study considers three distinct types of lacunarity to accommodate the nature of our data. First, we introduce binary lacunarity (T_LAC), where cells can only have values of 0 or 1. Furthermore, we explore stretched lacunarity (T_LAC_S), where values greater than one are spread across multiple cells, reflecting a stretched representation. Finally, we

employ weighted lacunarity (T_LAC_W), preserving cells with values greater than one in their original form (i.e., assigning to each cell t_p a value equal to the number of pixel with time tag t_p).

Temporal coherence. It is a measure of the monotonicity of the shower evolution in space and time. Pixels are arranged in a time-ordered sequence (earliest to latest). For each of them, we evaluate the spatial distance from the one with the earliest time. To this distance (d_p), we assign a negative sign if it is lower than the one evaluated for the previous pixel, otherwise, d_p is defined as positive. The parameter of interest is then defined as $T\_COHER = \sum d_p$, with the signs as defined above: higher values correspond to a more ordered development of the image.

Figures 2 and 3 show the distribution of the most promising parameters in different SIZE ranges.

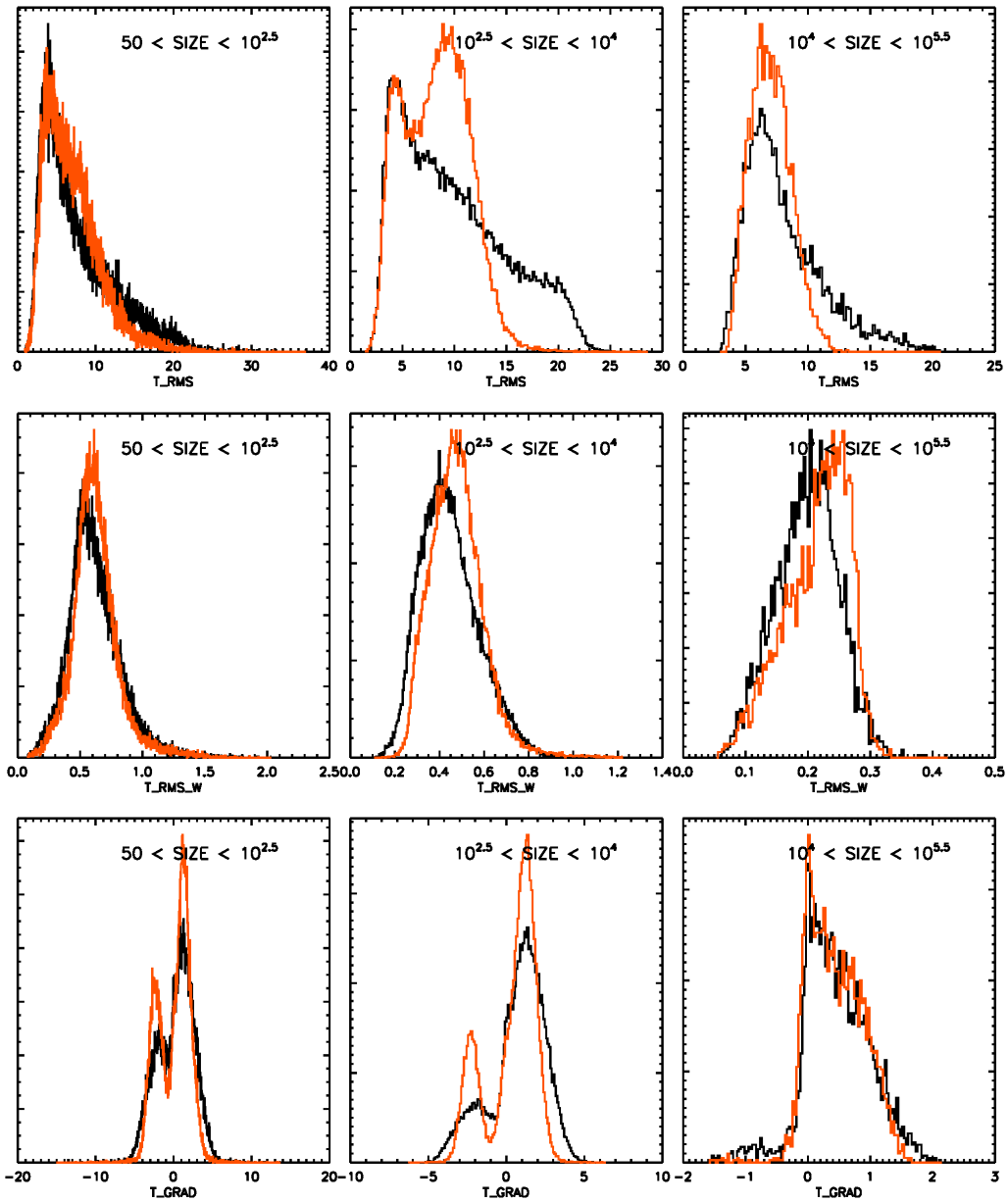

Figure 2. *Cont.*

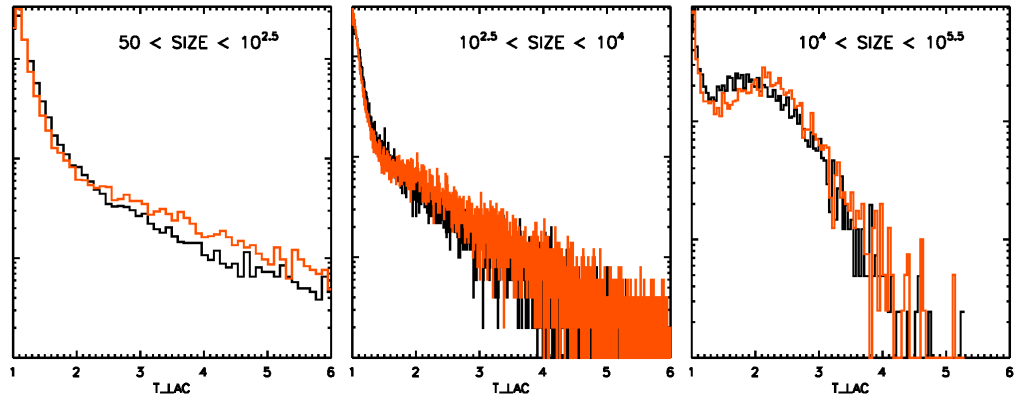

Figure 2. Distribution of selected time parameters in the Gamma-ray (black curve) and proton (orange curve) samples in different SIZE ranges.

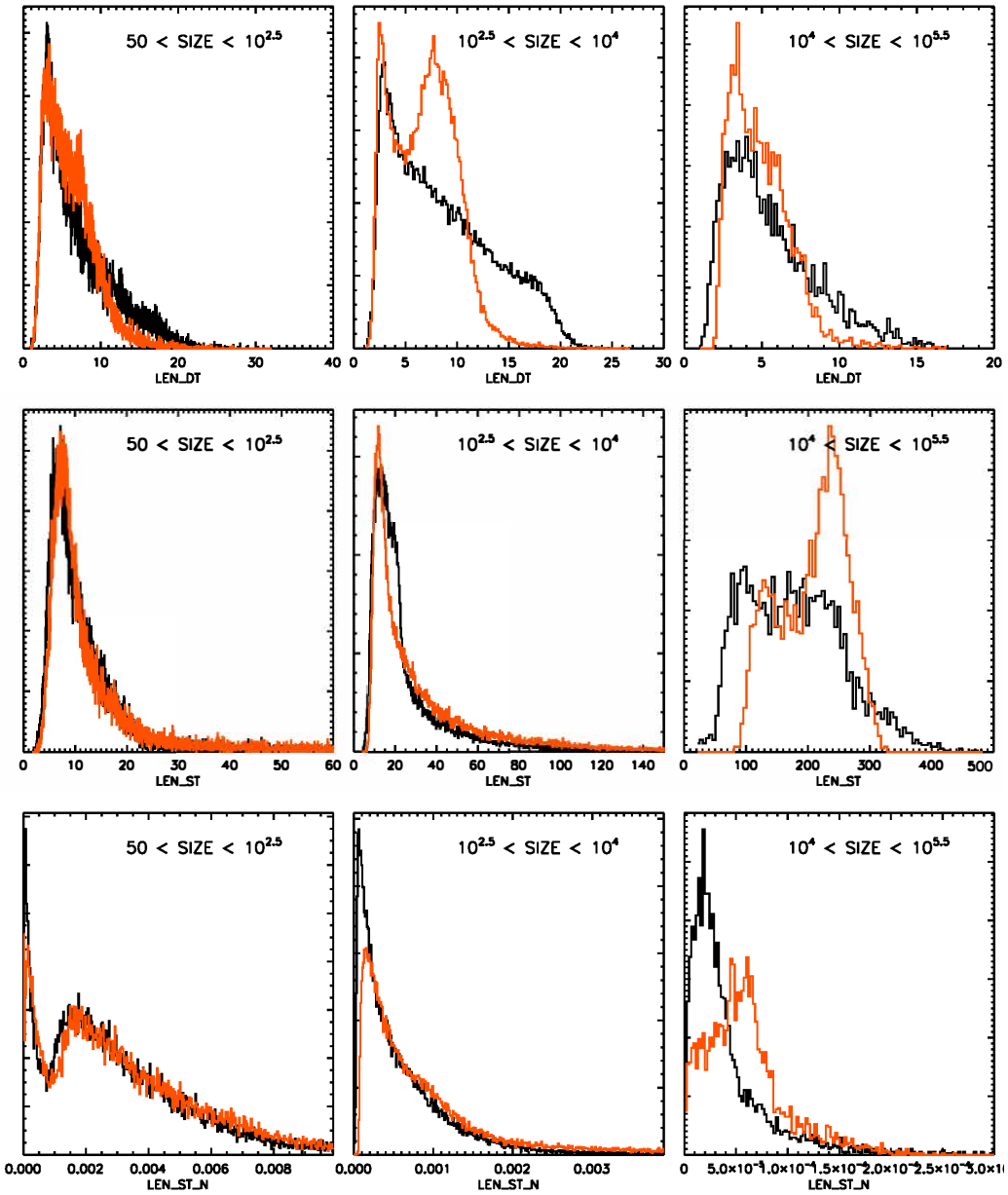

Figure 3. *Cont.*

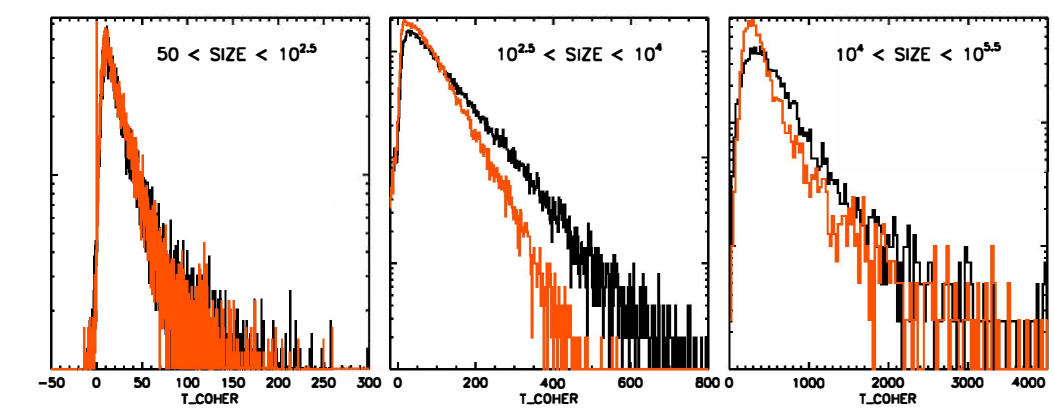

Figure 3. Distribution of time parameters in the Gamma-ray (black curve) and proton (orange curve) samples in different SIZE ranges.

5. Time Parameter Selection

In order to optimize the selection of the temporal parameters to be included in the analysis, we have performed a correlation analysis that allows us to identify and exclude redundant parameters. The correlation matrix presented in Figure 4 illustrates the relationships between various temporal parameters considered in our study. The correlations range from -1 to 1, where 1 indicates a perfect positive correlation, -1 a perfect negative correlation, and 0 no correlation.

The network graph in Figure 5 provides a visual representation of the correlations among the temporal parameters, highlighting the strength and direction of the relationships.

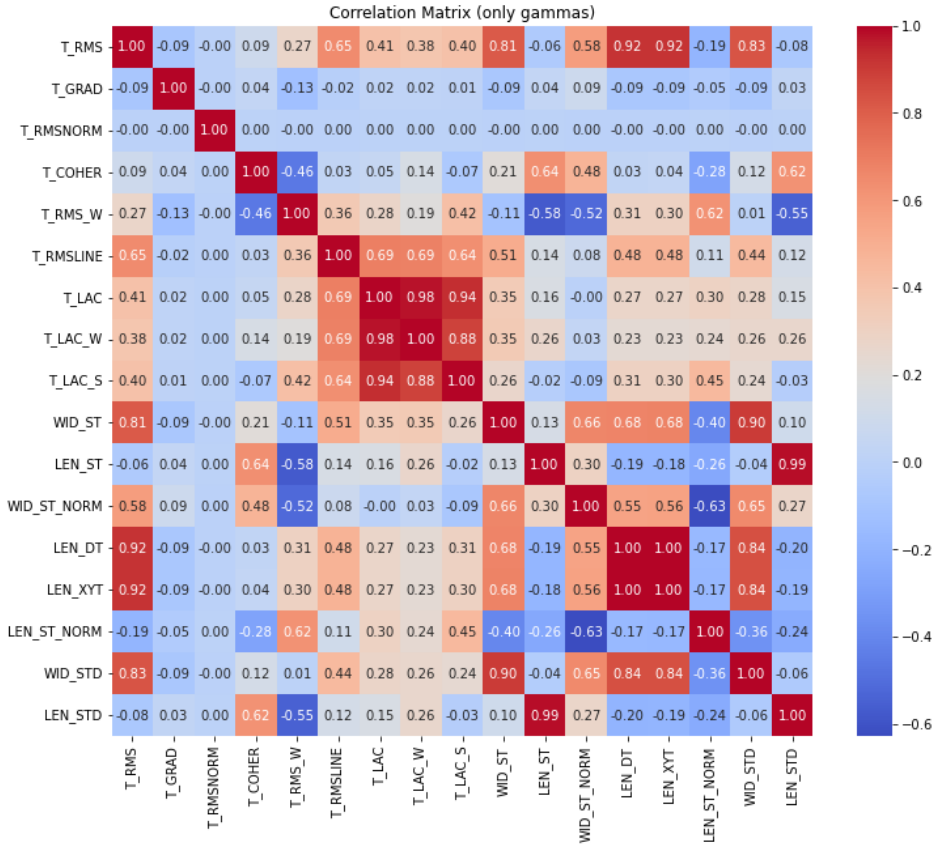

Figure 4. Correlation matrix of the temporal parameters.

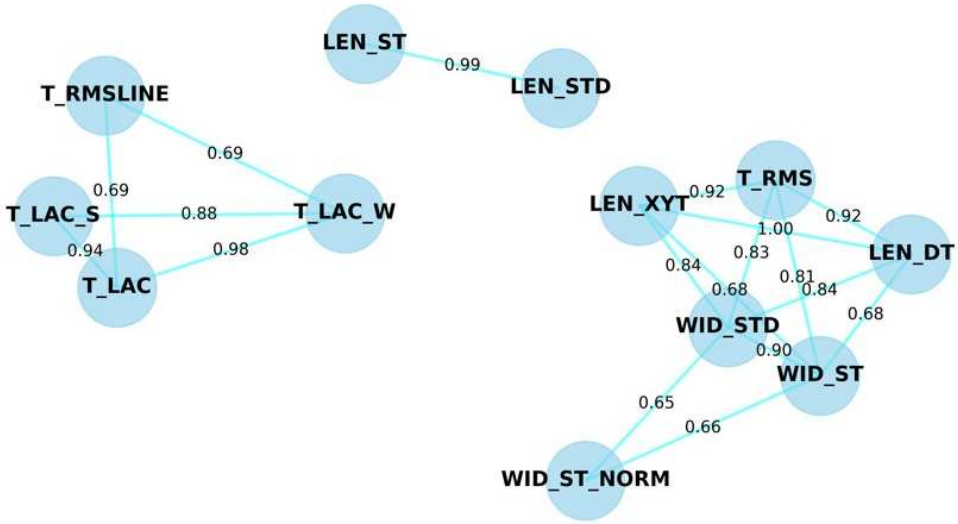

Figure 5. Network graph of the temporal parameter correlations.

The matrix highlights several strong correlations among the parameters. For example, *T_LAC_W* and *T_LAC* show a near perfect correlation (0.98), suggesting that these parameters provide similar information about the temporal structure of Cherenkov showers. Similarly, *LEN_ST* and *LEN_ST_NORM* also show a very high correlation (0.99), indicating redundancy between these measures.

Our feature selection approach focused on systematic redundancy elimination while preserving discriminatory power. When faced with highly correlated parameter pairs (correlation coefficient > 0.90), we retained only one parameter from each strongly correlated cluster. Our selection prioritized parameters with higher feature importance scores in preliminary Random Forest models and those with lower computational complexity. For example, between *T_LAC_W* and *T_LAC*, we selected *T_LAC* due to its marginally higher importance ranking and simpler computational requirements.

The final set of eight time parameters was determined through an iterative process that balanced four key criteria:

- **Diversity in Information**: The chosen parameters cover a broad range of temporal characteristics, from dispersion distributions to time gradients and coherence, ensuring comprehensive representation of shower temporal dynamics.
- **Low Redundancy**: Parameters with high correlations to others were excluded to retain only unique and independent features that contribute distinctly to the model's predictive power.
- **Feature Importance**: Selected parameters exhibit significant importance scores that justify their inclusion. As shown in the Random Forest feature importance plot (Figure 6), *LEN_DT* and *LEN_ST* are among the top features, indicating their strong predictive power in gamma/hadron separation.
- **Practical Considerations**: We preferred parameters that are easier to compute and interpret, such as *T_RMS* and *LEN_DT*, over more complex three-dimensional parameters. This pragmatic approach ensures that the model remains efficient for real-time data analysis.

While we considered dimensionality reduction techniques such as Principal Component Analysis (PCA), we ultimately opted for direct parameter selection to maintain physical interpretability of the features. This approach preserves the direct connection between each parameter and its underlying physical meaning, which is particularly valuable for understanding the temporal evolution of gamma-ray versus hadron-induced showers.

The application of these criteria resulted in the selection of eight parameters optimized for Gamma/Hadron separation.

- *T_RMS* (Root Mean Square of pixel trigger times): This parameter provides information on the dispersion of the arrival times of Cherenkov photons, which is useful in distinguishing between the more regular photon-induced showers and the more irregular hadron-induced showers.
- *T_GRAD* (gradient of arrival times): This measures the time gradient across the camera, helping to identify the shower orientation and differentiate between gamma and hadron events.
- *T_COHER* (coherence of the arrival times): This parameter assesses the temporal coherence of the Cherenkov photons, with gamma-ray showers typically exhibiting higher coherence compared to hadron-induced showers.
- *T_RMS_W* (weighted RMS of arrival times): This is a weighted version of *T_RMS*, which accounts for the intensity of the signal, providing a refined measure of the temporal spread.
- *T_LAC* (lacunarity of the arrival times sequence): This parameter captures the degree of homogeneity in arrival times, with a sparser distribution that can be indicative of hadron showers.
- *LEN_ST* (length of shower in time): This parameter measures the temporal extent of the shower, helping to differentiate between the typically shorter gamma-ray showers and the longer hadron-induced ones.
- *LEN_DT* (delta time length): This parameter represents the difference in time length across different parts of the shower, providing insights into the temporal asymmetry of the event.
- *LEN_ST_NORM* (normalized shower length in time): This is a normalized version of *LEN_ST*, offering a dimensionless measure that aids in comparing showers of different sizes and intensities.

Figures 7 and 8 compare the feature importance of different sets of parameters. Specifically, Figure 7 shows the case where only morphological and stereoscopic parameters are used, without any temporal parameters, achieving a quality factor (QF) of 3.32. The quality factor is defined as $QF = \frac{\epsilon_\gamma}{\sqrt{1-\epsilon_h}}$, where ϵ_γ and ϵ_h are, respectively, the number of correctly identified gamma events and the number of correctly identified hadron events. Figures 6 and 8 then compare the importance when using all temporal parameters versus a selected subset. The QF increases from 3.65 when using all temporal parameters to 3.68 when using only the selected parameters. This improvement indicates that the selected parameters not only reduce computational complexity, but also enhance model performance.

The correlation matrix (Figure 4), network graph (Figure 5) and feature importance plots (Figures 7 and 8) included in this paper visually support the selection rationale and underscore the efficacy of these parameters in our machine learning models. The integration of these features is anticipated to significantly enhance the discrimination between gamma-ray and hadron showers, contributing to the overall performance of the IACT system. The integration of these temporal parameters into the rejection algorithm significantly improves its performance, as evidenced by the increased Quality Factor (QF) from 3.32 to 3.68, representing an increase of approximately 10.8%. This enhancement underscores the value of these parameters in effectively distinguishing between gamma and hadron events, thereby optimizing the analysis performance.

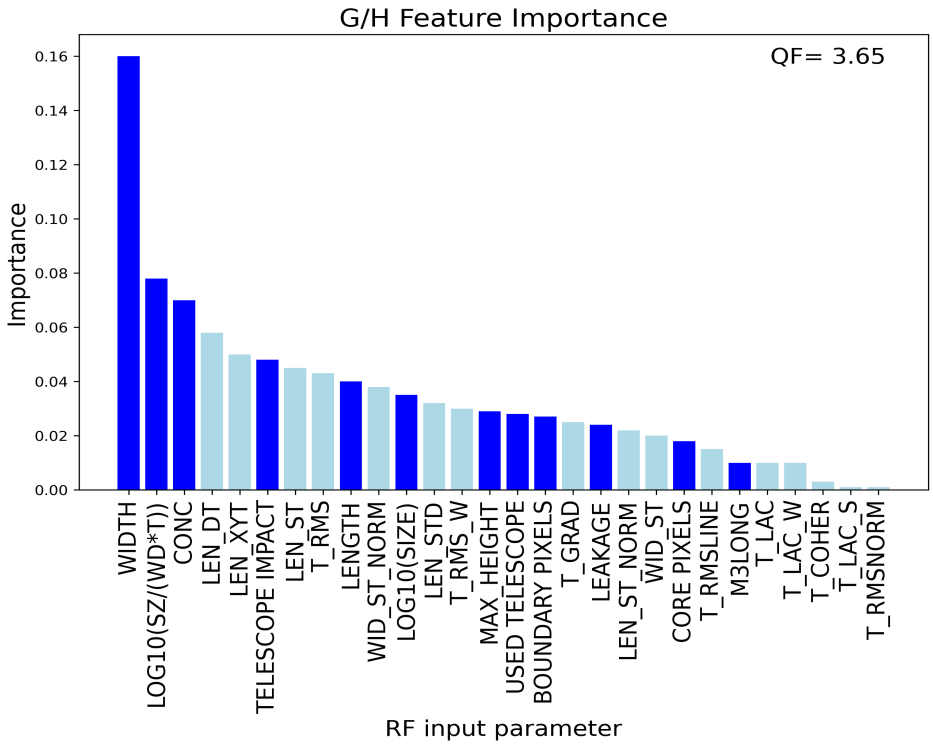

Figure 6. Feature importance of morphological, stereo, and all temporal parameters using random forest (blue for morphological and stereo parameters, light blue for temporal parameters).

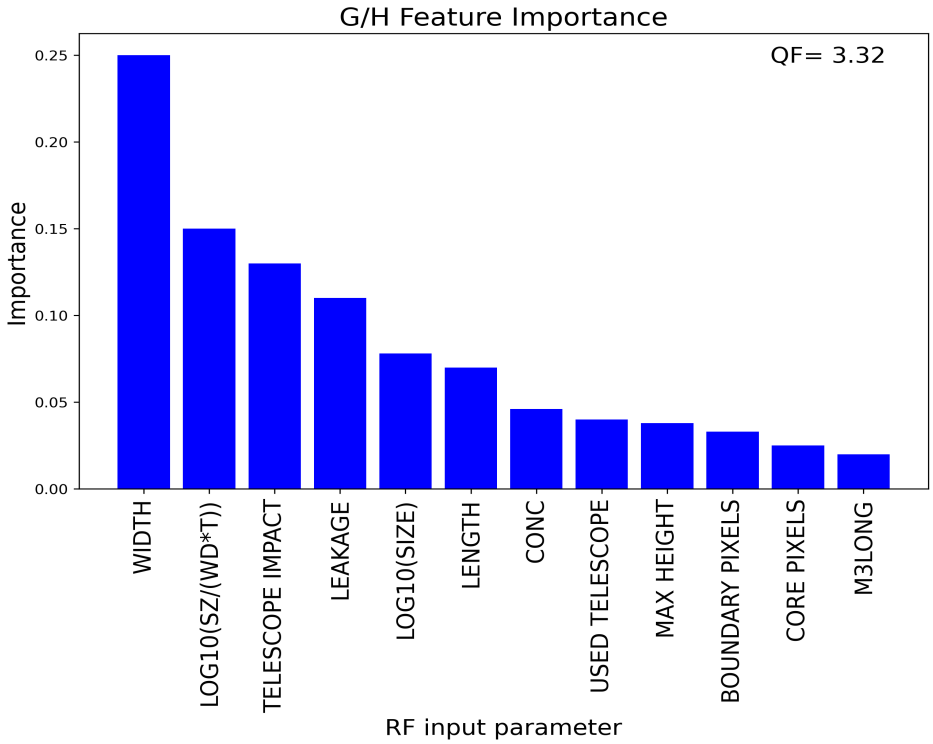

Figure 7. Feature importance of morphological and stereo parameters without any temporal parameters using random forest.

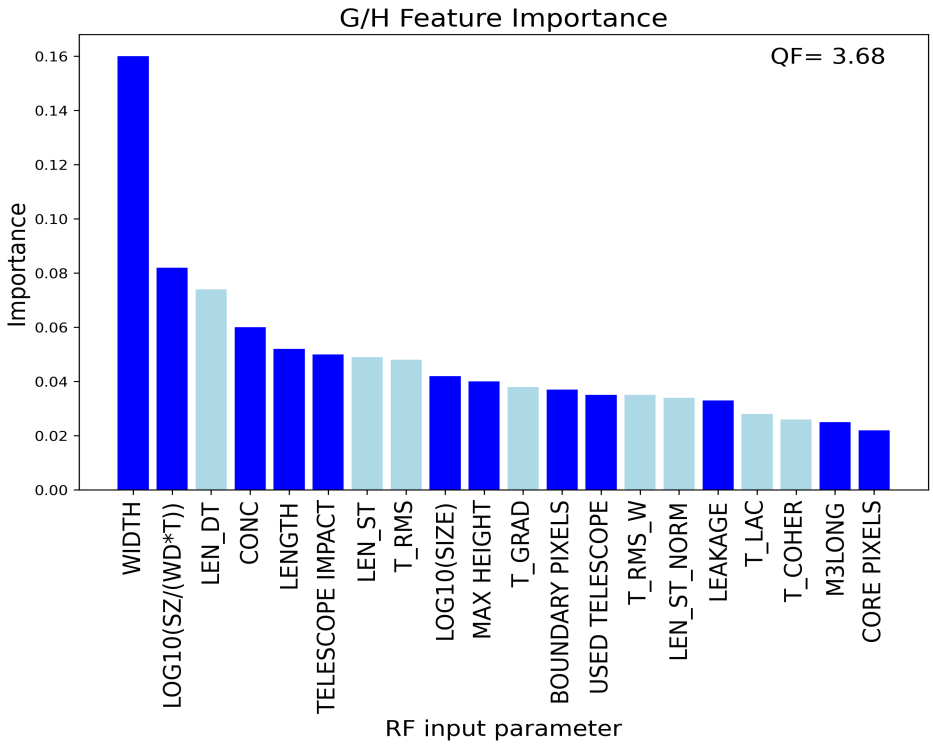

Figure 8. Feature importance of morphological, stereo, and selected temporal parameters using random forest (blue for morphological and stereo parameters, light blue for temporal parameters).

6. High-Level Performance

In order to provide a final high-level assessment of the performance of the temporal parameters investigated in this work, we derived the main performance metrics using the standard routine implemented in the ASTRI pipeline [9]. We evaluated the efficiency of the Gamma/Hadron discrimination algorithm implemented in `A-SciSoft` both with the standard set of parameters and with the inclusion of temporal parameters, and compared the two resulting datasets in terms of differential flux sensitivity (for an exposure time of 50 h), energy resolution, and angular resolution. A detailed study on the impact of temporal parameters in the energy reconstruction procedure will be addressed in a future work.

We incorporated temporal parameter analysis into the DL2a processing pipeline, using the complete Monte Carlo dataset outlined in Section 2. The analysis spans an energy range from $10^{-0.5}$ TeV ($\simeq$0.3 TeV) to $10^{2.5}$ TeV ($\simeq$300 TeV). To ensure realistic representation of actual source observations, we implemented an energy-dependent event weighting scheme for both background (proton) and gamma-ray events in the Level 2b (DL2b) samples. The weighting procedure follows the methodology established in [30]. For gamma-ray events, we applied weights derived from the well-established Crab Nebula spectrum measured by the HEGRA Collaboration [31], which serves as a standard reference source in very high-energy gamma-ray astronomy. This approach ensures that our analysis reflects realistic spectral distributions encountered in observational data.

For completeness in our high-level analysis, we included the electron-induced background events, although their contribution to the irreducible gamma-like background is minimal at the ASTRI Mini-Array's primary operational energies (E > $\sim$1 TeV). At these energies, proton-initiated showers overwhelmingly dominate the background component.

Our analysis protocol implements a multi-parameter selection framework applied to the Level 2b (DL2b) samples, incorporating three primary criteria:

- Background rejection efficiency ("gammaness");
- Shower arrival direction reconstruction;

- Event multiplicity thresholds.

These selection criteria were optimized independently within each energy bin to maximize sensitivity for a 50 h exposure time. For event acceptance, we required a detection significance of 5σ (calculated according to Equation (17) in [32]) within each energy bin, maintaining consistent exposure parameters with the optimization phase.

The analysis methodology employs an on-source/off-source approach, with an off-source to on-source exposure ratio of 5. This approach is fundamental to Cherenkov telescope data analysis: gamma-ray signals in the "on-source" region must be evaluated against "off-source" background control regions. For point-source observations, the data acquisition strategy enables the definition of multiple background control regions (typically 5) with identical acceptance characteristics to the signal region, ensuring reliable background estimation. Additional quality criteria included the following:

- Minimum signal excess threshold of 10 events;
- Signal-to-systematic uncertainty ratio exceeding 5:1 (assuming 1% systematic uncertainty in background estimation).

These selection criteria align with established IACT community standards [30], enabling performance evaluation under well-defined and reproducible analysis conditions.

Figure 9 shows the on-axis point-like source differential sensitivity (in 50 h) achieved with the use of a standard set of morphological and stereoscopic parameters for gamma/hadron separation computation (blue points) and with the additional use of the temporal parameters investigated in this work (orange points). The ratios between the results of the two methods are also shown.

As apparent in Figures 9–11, the inclusion of the temporal parameters in the gamma/hadron rejection algorithm causes a significant improvement (up to ∼50%) of the array sensitivity in the energy range below ∼1.5 TeV, while above that energy, the two analyses provide basically the same results.

On the other hand, there is no comparable improvement, but no deterioration either, in energy or angular resolution. This was somewhat expected as for the energy and arrival direction reconstruction we used for any high-level analysis the standard reconstruction procedure implemented in `A-SciSoft`, which does not use any time parameters related information [14].

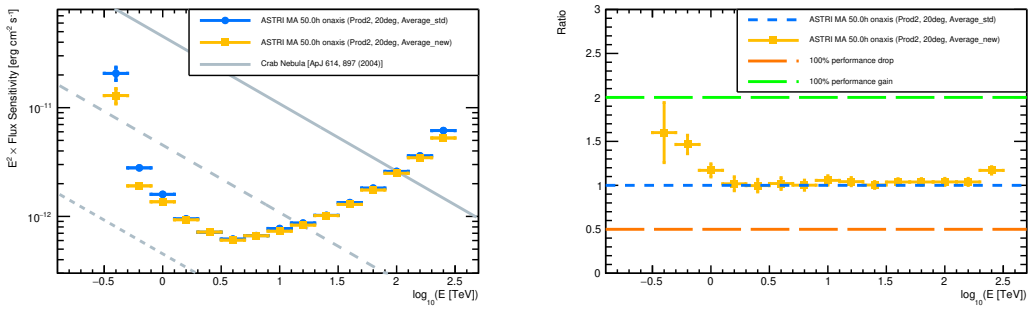

Figure 9. (**left**) On-axis differential sensitivity (in 50 h) achieved with the inclusion of the temporal parameters, apart from the standard morphological and stereoscopic ones, in the gamma/hadron separation procedure (orange points) against the benchmark method (i.e., with the use of standard morphological and stereoscopic parameters only, blue points) For the solid grey line [33]. (**right**) Ratio between the on-axis differential sensitivities achieved from the two different analyses. Higher values correspond to better performance.

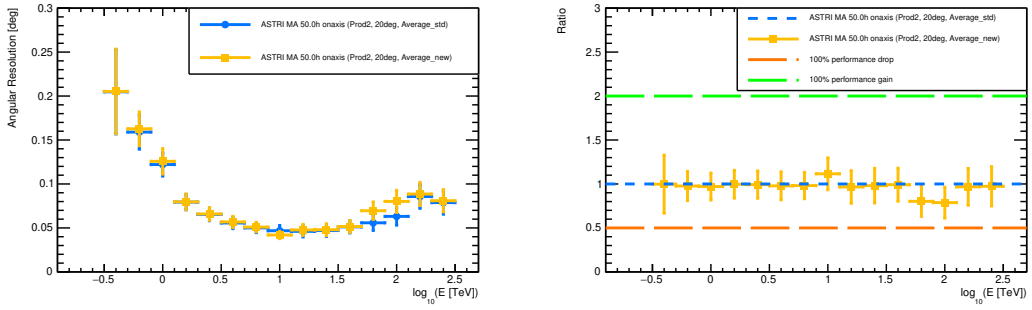

Figure 10. (**left**) On-axis angular resolution achieved with the inclusion of the temporal parameters, apart from the standard morphological and stereoscopic ones, in the gamma/hadron separation procedure (orange points) against the benchmark method (i.e., with the use of standard morphological and stereoscopic parameters only, blue points). (**right**) Ratio between the on-axis angular resolutions achieved from the two different analyses. Lower values correspond to better performance.

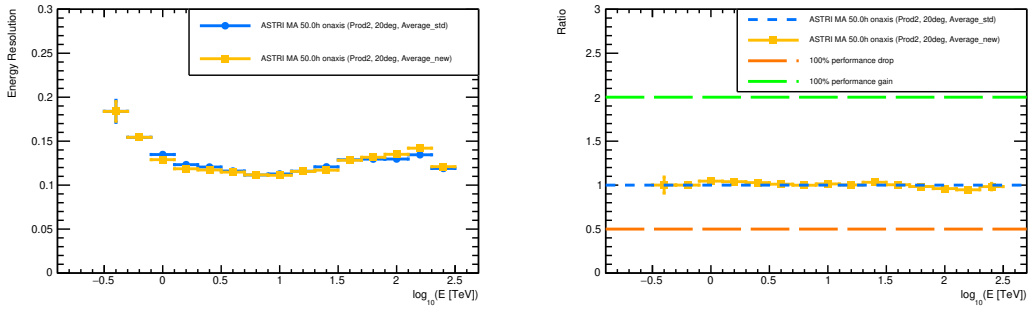

Figure 11. (**left**) On-axis energy resolution achieved with the inclusion of the temporal parameters, apart from the standard morphological and stereoscopic ones, in the gamma/hadron separation procedure (orange points) against the benchmark method (i.e., with the use of standard morphological and stereoscopic parameters only, blue points). (**right**) Ratio between the on-axis energy resolutions achieved from the two different analyses. Lower values correspond to better performance.

7. Discussion and Conclusions

This study presents a comprehensive analysis of the integration of temporal parameters into the gamma/hadron separation algorithm used in the context of the ASTRI Mini-Array Imaging Atmospheric Cherenkov Telescopes (IACTs). Our primary objective was to enhance the discrimination capabilities between gamma-ray and hadron-induced showers by selecting a subset of temporal parameters that provide unique and complementary information about the temporal dynamics of the Cherenkov showers.

The correlation analysis revealed significant relationships among various temporal parameters, allowing us to identify and exclude redundant features. By carefully selecting eight key parameters—T_RMS, T_GRAD, T_COHER, T_RMS_W, T_LAC, LEN_ST, LEN_DT, and LEN_ST_NORM—we were able to capture diverse aspects of the shower characteristics, ultimately improving the model's performance.

The introduction of these temporal parameters into the Random Forest (RF) model resulted in a notable enhancement of the gamma/hadron separation, as evidenced by the increase in the Quality Factor (QF) from 3.32 to 3.68, representing an improvement of approximately 10.8% compared to the current procedure implemented in `A-SciSoft` and used as a benchmark. This improvement underscores the effectiveness of the selected parameters in refining the discrimination process.

Although the improvement is concentrated only at the lowest energies, the result is to be considered promising in every way for observations for which the lowest energies

are particularly important, such as observations of transients and, in general, of extragalactic objects.

The more pronounced impact of temporal parameters at lower energies (below ∼1.5 TeV) can be attributed to several key factors. At these energies, the Cherenkov showers tend to be less developed and have lower photon densities, making the morphological differences between gamma and hadron events more subtle. The temporal evolution of the shower becomes particularly important in this regime as it provides complementary information that the standard morphological parameters alone cannot effectively capture. Additionally, at lower energies, the shorter duration and more coherent development of gamma-ray induced showers stands in greater contrast to the more chaotic temporal structure of hadron showers. This temporal distinction becomes less pronounced at higher energies, where both shower types produce stronger signals with more defined morphological characteristics, making the traditional spatial parameters alone sufficient for effective discrimination.

In addition, it is worth noting that the impact of temporal parameters in gamma/hadron separation is expected to be much more efficient in the case of observations performed by a single telescope, since in this case the stereoscopic parameters are not accessible. The study of this use case, which is particularly important in view of the first ASTRI Mini-Array telescope observations (already ongoing), may be considered in future work.

Future work could focus on further refining these parameters and exploring their potential interactions with other features to uncover additional performance gains. It is worth noting that in this study, the temporal parameters were tested only with the Random Forest model. However, our future work aims to investigate the application of more advanced ensemble learning models, such as those presented in [4], to the temporal parameters. This will allow us to explore the potential benefits of combining advanced machine learning techniques with the temporal parameters, building on the promising results already obtained with morphological and stereo parameters. In addition to exploring more advanced ensemble learning models, we plan to investigate deep learning approaches for gamma/hadron discrimination using temporal parameters. While Random Forests provide interpretable results and good performance with manageable computational costs, deep neural networks—particularly convolutional or recurrent architectures—might capture more complex temporal patterns in the shower development. Such networks could potentially extract hierarchical features directly from the raw time and intensity data without requiring manual feature engineering. However, this would need to be balanced against the increased computational demands and reduced interpretability inherent to deep learning models. A comparative study between our Random Forest approach and various deep learning architectures would provide valuable insights for the IACT community.

Author Contributions: Conceptualization, V.L.P., G.C., S.L., A.L.B., A.T. and A.P.; Methodology, V.L.P., G.C., S.L., A.A.C., A.L.B., A.T. and A.P.; Software, V.L.P., S.L., A.A.C., A.T. and A.P.; Validation, V.L.P., S.L., A.A.C., A.T. and A.P.; Formal analysis, V.L.P., S.L. and A.P.; Investigation, V.L.P., S.L. and A.P.; Resources, V.L.P.; Data curation, V.L.P., S.L. and A.P.; Writing—original draft, V.L.P., S.L. and A.P.; Writing—review & editing, V.L.P., S.L. and A.P.; Visualization, V.L.P. and A.P.; Supervision, V.L.P., S.L., A.L.B. and A.P.; Funding acquisition, V.L.P., S.L. and A.P. All authors have read and agreed to the published version of the manuscript.

Funding: This work is partially supported by ICSC—Centro Nazionale di Ricerca in High Performance Computing, Big Data and Quantum Computing, funded by European Union—NextGenerationEU. We acknowledge financial support from the ASI-INAF agreement n. 2022-14-HH.0.

Institutional Review Board Statement: Not applicable.

Informed Consent Statement: Not applicable.

Data Availability Statement: The data presented in this study are available on request from the corresponding author. The data are not publicly available due to ASTRI experiment simulation data policy.

Acknowledgments: This work was conducted in the context of the ASTRI Project. We gratefully acknowledge support from the people, agencies, and organisations listed here: http://www.astri.inaf.it/en/library/ accessed on 1 March 2025. This work is partially supported by ICSC—Centro Nazionale di Ricerca in High Performance Computing, Big Data and Quantum Computing, funded by European Union—NextGenerationEU. We acknowledge financial support from the ASI-INAF agreement n. 2022-14-HH.0. This paper went through the internal ASTRI review process.

Conflicts of Interest: The authors declare no conflicts of interest.

References

1. de Naurois, M.; Mazin, D. Ground-based detectors in very-high-energy gamma-ray astronomy. *Comptes Rendus Phys.* **2015**, *16*, 610–627.
2. Stanev, T. *High Energy Cosmic Rays*, 2nd ed.; Springer Praxis Books; Springer: Berlin/Heidelberg, Germany, 2010.
3. Hillas, A.M. Cherenkov light images of EAS produced by primary gamma rays and by nuclei. In Proceedings of the 19th International Cosmic Ray Conference, San Diego, CA, USA, 11–23 August 1985; NASA, Goddard Space Flight Center: Washington, DC, USA, 1985; pp. 445–448.
4. Pagliaro, A.; Cusumano, G.; La Barbera, A.; La Parola, V.; Lombardi, S. Application of Machine Learning Ensemble Methods to ASTRI Mini-Array Cherenkov Event Reconstruction. *Appl. Sci.* **2023**, *13*, 8172. [CrossRef]
5. Heß, M.; Bernlöhr, K.; Daum, A. Monte Carlo studies of the imaging atmospheric Cherenkov technique for the detection of gamma-rays above 10 GeV. *Astropart. Phys.* **1999**, *11*, 363.
6. de la Calle Pérez, I.; Biller, S.D. Differential sensitivity of high-energy gamma-ray telescopes. *Astropart. Phys.* **2006**, *26*, 69.
7. Aliu, E.; Anderhub, H.; Antonelli, L.A. Performance of the MAGIC telescopes in stereoscopic mode for gamma-ray astronomy observations above 50 GeV energy threshold. *Astropart. Phys.* **2009**, *30*, 293–305.
8. Scuderi, S.; Giuliani, A.; Pareschi, G.; Tosti, G.; Catalano, O.; Amato, E.; Antonelli, L.A.; Gonzàles, J.B.; Bellassai, G.; Bigongiari, C.; et al. The ASTRI Mini-Array of Cherenkov Telescopes at the Observatorio del Teide. *J. High Energy Astrophys.* **2022**, *35*, 52–68.
9. Lombardi, S.; Antonelli, L.A.; Bigongiari, C.; Cardillo, M.; Gallozzi, S.; Green, J.G.; Lucarelli, F.; Saturni, F.G. Performance of the ASTRI Mini-Array at the Observatorio del Teide. In Proceedings of the 37th International Cosmic Ray Conference, Berlin, Germany, 12–23 July 2021; p. 884.
10. Vercellone, S.; Bigongiari, C.; Burtovoi, A.; Cardillo, M.; Catalano, O.; Franceschini, A.; Lombardi, S.; Nava, L.; Pintore, F.; Stamerra, A.; et al. ASTRI Mini-Array core science at the Observatorio del Teide. *J. High Energy Astrophys.* **2022**, *35*, 1.
11. Pareschi, G. The ASTRI SST-2M prototype and mini-array for the Cherenkov Telescope Array (CTA). *Proc. SPIE* **2016**, *9906*, 99065T.
12. Lombardi, S.; Catalano, O.S.; Scuderi, S.; Antonelli, L.A.; Pareschi, G.; Antolini, E.; Arrabito, L.; Bellassai, G.; Bernlöhr, K.; Bigongiari, C.; et al. First detection of the Crab Nebula at TeV energies with a Cherenkov telescope in a dual-mirror Schwarzschild-Couder configuration: The ASTRI-Horn telescope. *Astron. Astrophys.* **2020**, *634*, A22.
13. Giro, E.; Canestrari, R.; Sironi, G.; Antolini, E.; Conconi, P.; Fermino, C.E.; Gargano, C.; Rodeghiero, G.; Russo, F.; Scuderi, S.; et al. First optical validation of a Schwarzschild Couder telescope: The ASTRI SST-2M Cherenkov telescope. *Astron. Astrophys.* **2017**, *608*, A86.
14. Lombardi, S.; Antonelli, L.A.; Bigongiari, C.; Cardillo, M.; Lucarelli, F.; Perri, M.; Stamerra, A.; Visconti, F. ASTRI data reduction software in the framework of the Cherenkov Telescope Array. In Proceedings of the Software and Cyberinfrastructure for Astronomy V, Proceedings of the SPIE Astronomical Telescopes + Instrumentation, Austin, TX, USA, 10–15 June 2018 ; Volume 10707, p. 107070R.
15. Breiman, L. Random Forests. *Mach. Learn.* **2001**, *45*, 5–32. [CrossRef]
16. Zanin, R. MARS, the MAGIC Analysis and Reconstruction Software. In Proceedings of the International Cosmic Ray Conference, Rio de Janeiro, Brazil, 2–9 July 2013; p. 2937.
17. Lombardi, S. Advanced stereoscopic gamma-ray shower analysis with the MAGIC telescopes. In Proceedings of the International Cosmic Ray Conference, Beijing, China, 11–18 August 2011; p. 266.
18. Spencer, S.; Armstrong, T.; Watson, J.; Mangano, S.; Renier, Y.; Cotter, G. Deep learning with photosensor timing information as a background rejection method for the Cherenkov Telescope Array. *Astropart. Phys.* **2021**, *129*, 102579. [CrossRef]
19. Holder, J. Exploiting VERITAS timing information. In Proceedings of the 29th International Cosmic Ray Conference (ICRC29), Pune, India, 3–10 August 2005; p. 383.

20. Chalmé-Calvet, R.; Holler, M.; de Naurois, M.; Tavernet, J.P. Exploiting the time of arrival of Cherenkov photons at the 28 m H.E.S.S. telescope for background rejection: Methods and performance. In Proceedings of the 34th International Cosmic Ray Conference (ICRC2015), The Hague, The Netherlands, 30 July–6 August 2015; p. 842.
21. Heck, D.; Knapp, J.; Capdevielle, J.N.; Schatz, G.; Thouw, T. *CORSIKA: A Monte Carlo Code to Simulate Extensive Air Showers*; Report FZKA, 6019; Forschungszentrum Karlsruhe: Karlsruhe, Germany, 1998.
22. Bernlöhr, K. Simulation of imaging atmospheric Cherenkov telescopes with CORSIKA and sim telarray. *Astropart. Phys.* **2008**, *30*, 149. [CrossRef]
23. Pence, W.D.; Chiappetti, L.; Page, C.G.; Shaw, R.A.; Stobie, E. Definition of the Flexible Image Transport System (FITS), version 3.0. *Astron. Astrophys.* **2010**, *524*, A42. [CrossRef]
24. Sottile, G.; Sangiorgi, P.; Gargano, C.; Gerfo, L.; Corpora, M.; Catalano, O.; Impiombato, D.; Mollica, D.; Capalbi, M.; Mineo, T. Design and characterization of a novel Cherenkov telescope array for gamma-ray astronomy: The ASTRI Mini-Array project. *arXiv* **2023**, arXiv:2301.09915.
25. Hillas, A.M.; Akerlof, C.W.; Biller, S.D.; Buckley, J.H.; Carter-Lewis, D.A.; Catanese, M.; Cawley, M.F.; Fegan, D.J.; Finley, J.P.; Gaidos, J.A.; et al. The spectrum of TeV gamma rays from the Crab Nebula. *Astrophys. J.* **1998**, *503*, 744–759. [CrossRef]
26. Mandelbrot, B.B. *The Fractal Geometry of Nature*; W.H. Freeman: New York, NY, USA, 1983.
27. Lin, B.; Yang, Z.R. Critical exponents of percolation transition in fractal structures. *J. Phys. A* **1986**, *19*, L49. [CrossRef]
28. Gefen, Y.; Meir, Y.; Aharony, A. Scaling properties of random systems near criticality: Fractal dimensionality and percolation theory. *Phys. Rev. Lett.* **1983**, *50*, 145.
29. Allain, C.; Cloitre, M. Characterizing the lacunarity of random and deterministic fractal sets. *Phys. Rev. A* **1991**, *44*, 3552. [CrossRef]
30. Acharya, B.S. Science with the Cherenkov Telescope Array (CTA). *Astropart. Phys.* **2019**, *111*, 35. [CrossRef]
31. Aharonian, F.A.; Akhperjanian, A.G.; Barrio, J.A.; Bernlöhr, K.; Bojahr, H.; Calle, I.; Contreras, J.L.; Cortina, J.; Daum, A.; Deckers, T.; et al. The Energy spectrum of TeV gamma-rays from the Crab nebula as measured by the HEGRA system of imaging air Cherenkov telescopes. *Astrophys. J.* **2000**, *539*, 317–324.
32. Li, T.-P.; Ma, Y.-Q. Analysis methods for results in gamma-ray astronomy using statistical significance testing techniques. *Astrophys. J* **1983**, *272*, 317.
33. Aharonian, F.; Akhperjanian, A.; Beilicke, M.; Bernlöhr, K.; Börst, H.-G.; Bojahr, H.; Bolz, O.; Coarasa, T.; Contreras, J.L.; Cortina, J.; et al. The Crab Nebula and Pulsar between 500 GeV and 80 TeV: Observations with the HEGRA Stereoscopic Air Cerenkov Telescopes. *Astrophys. J.* **2004**, *614*, 897–913.